Multiscale Maxwell–Schrödinger modeling: A split field finite-difference time-domain approach to molecular nanopolaritonics

Kenneth Lopata and Daniel Neuhauser[a)]
Department of Chemistry and Biochemistry, University of California, Los Angeles, California 90095-1569, USA

(Received 11 November 2008; accepted 26 January 2009; published online 12 March 2009)

We present a combined finite-difference time-domain/linear response approach for modeling plasmon/molecule systems. The self-interaction of the molecule is avoided by splitting the fields and currents into two parts: those due to the molecule and those from everything else. This approach is suitable for describing surface plasmons on metal nanostructures interacting in the near field with nearby dipolar molecules or semiconductor nanostructures. The approach is applied to three collinear 5 nm diameter gold nanoparticles; the results demonstrate that a nearby molecule strongly affects surface plasmon transfer along the array. Specifically, an *xy* oriented molecule situated midway between the second and third nanoparticles exhibits a symmetric Fano-type inference effect. Transmission of incident *x*-polarized energy from the second nanoparticle to the third is enhanced over a frequency range below the molecular resonance, and partially scattered into *y*-polarized currents for frequencies above. At the molecule's resonance frequency, the magnitude of the resulting *y*-current is approximately 20% of the *x*-current. © *2009 American Institute of Physics*. [DOI: 10.1063/1.3082245]

I. INTRODUCTION

Molecular nanopolaritonics,[1] the study of the near-field interactions between surface plasmons and nearby dipolar matter such as molecules and semiconductor nanostructures, has been the focus of much research interest. Broadly speaking, the applications of these near-field plasmon/matter interactions are twofold. On one hand, plasmonic structures[2,3] are routinely used to focus electromagnetic energy at subwavelength scales into matter. For example, the strong fields around the surface of metal nanoparticles are exploited in surface enhanced Raman spectroscopy to significantly boost sensitivity to dilute concentrations of analyte molecules[4–6] or to enhance emission of fluorescent molecules.[7,8] On the other hand, dipolar dynamics can induce surface plasmons on metals, such as when molecular excitations are nonradiatively damped near the surface of a metal structure.[9–11] Additionally, experimental and theoretical studies have demonstrated that dipolar material can, to some extent, control the propagation of surface plasmon-polariton (SPP) waves along metal nanostructures, such as linear arrays of gold nanoparticles,[1] silver hole arrays,[12] or through gold films.[13]

Some of the many approaches to modeling the interaction between plasmons and dipolar matter include point-plasmon/random phase approximation (RPA),[1] a combined Green's tensor/optical Bloch formalism,[14] multipole expansions,[11] and time-dependent density functional theory (TDDFT).[15,16] Many of these methods are either specific to a particular nanoparticle geometry (e.g., spheres) or can only treat relatively small systems. Any practical approach to large-scale modeling of arbitrary nanopolaritonic devices, however, must be generally applicable and have a good trade-off between accuracy and computational speed. The theoretical description of these systems is complicated, as combined plasmon/molecular systems involve multiple mechanisms and span a wide range of length scales from angstroms to nanometers to micrometers. A consistent formalism must describe both the electromagnetic and molecular excitations.

Metal structures, such as nanoparticles, films, and tips support surface plasmons in which a large number of free electrons in the conduction band undergo collection motion at the surface of the particle. For all but the smallest of metal clusters, the conduction band is continuous and plasmon motion is best described classically. Some methods for describing plasmonic systems include Mie scattering theory for spheres,[17,18] the discrete dipole approximation,[19,20] simplified excitonlike models,[21,22] hybridization approaches,[23,24] and the finite-difference time-domain (FDTD) method.[25–27] Among these, FDTD is one of the most powerful and versatile ways of calculating the time and space-resolved electric field, magnetic field, and currents in heterogeneous systems. In FDTD, the electric and magnetic fields are broken into two interlaced grids, and the system is evolved in a "leap-frog" style, where the electric field at a certain time is found from the magnetic field at the previous time and vice versa. The utility of this method is that it naturally gives the fields and currents in time and space, is easy to implement, and is highly accurate even on nanometer scales.[25]

The response of dipolar matter such as dye molecules, or even semiconductor nanostructures such as quantum dots, must be described quantum mechanically due to energy level discretization. A completely quantum mechanical treatment of the total system, however, using, for example, TDDFT is

[a)]Electronic mail: dxn@chem.ucla.edu.

prohibitively expensive computationally and can only be applied to extremely small systems of perhaps one or two small metal clusters and a few molecules, at most.

An efficient way to describe plasmon/molecule interactions is to treat the fields in the vacuum and metals classically and describe the optical response of the dipolar matter quantum mechanically. As a good first approximation, the molecular part of the system can be described using linear response, such as with the RPA, which is expected to be accurate in the limit of weak fields acting on the molecule. Linear response has the distinct advantage of capturing the basic physics of the molecular response without complicated formalism or computational burden. Note that models combining RPA for semiconductor nanoparticles and plasmons have been reported before,[28] as well as the combination of two-level molecules and photonics.[29]

This paper develops the full formalism for a merged FDTD-RPA approach, i.e., a combined Maxwell–Schrödinger description. This describes the system on two scales—a smaller one for the molecule and a larger one for the electrodynamic radiation. The key realization is to use two fields, one for the molecule and one for the plasmons, so that there are no singularities when calculating the electric fields; this is explained below.

In Sec. II we derive expressions for the FDTD evolution of the split electric fields, magnetic fields, and currents for a combined metal/molecule system, followed by an explanation of how to practically implement a combined FDTD-RPA approach. This is followed by simulation results in Sec. III, which demonstrate the strong effect a dipolar molecule has on near-field energy transfer through a chain of three gold spherical nanoparticles. A brief discussion of extensions to the formalism is presented in Sec. IV, and conclusions follow in Sec. V.

II. THEORY

In order to avoid self-interaction of the molecule with its own field, which is physically impossible for a two-level molecule, we need to split the total electric field, magnetic field, and current into two parts: one due to the molecule and one due to everything else (i.e., the vacuum and metal structures). We denote the fields from the molecule with an m (molecule) subscript and the fields due to everything else with an p (plasmonic) subscript. We similarly label the currents, remembering that the current from sources other than the molecule, comes only from metal structures in the system

$$\boldsymbol{E}_{\mathrm{tot}}(\boldsymbol{r},t)=\boldsymbol{E}_p(\boldsymbol{r},t)+\boldsymbol{E}_m(\boldsymbol{r},t), \tag{1}$$

$$\boldsymbol{H}_{\mathrm{tot}}(\boldsymbol{r},t)=\boldsymbol{H}_p(\boldsymbol{r},t)+\boldsymbol{H}_m(\boldsymbol{r},t), \tag{2}$$

$$\boldsymbol{J}_{\mathrm{tot}}(\boldsymbol{r},t)=\boldsymbol{J}_p(\boldsymbol{r},t)+\boldsymbol{J}_m(\boldsymbol{r},t). \tag{3}$$

A. Vacuum and metal part

First, we derive the FDTD evolution expressions for the parts of the fields and currents *not* due to the molecule, denoted as $\boldsymbol{E}_p(\boldsymbol{r},t)$, $\boldsymbol{H}_p(\boldsymbol{r},t)$, and $\boldsymbol{J}_p(\boldsymbol{r},t)$. Atomic units are used, which is equivalent to setting the electric constant $\epsilon_0=1/(4\pi)$, and the magnetic constant $\mu_0=1/(\epsilon_0 c^2)=4\pi/c^2$, where c is the speed of light in the vacuum, 137.04 a.u. Additionally, the background is the vacuum; extensions to dielectric backgrounds are straightforward. We start with the Maxwell's equations for the full fields and currents, which, neglecting magnetization effects in the metal, are

$$\frac{\partial \boldsymbol{E}_{\mathrm{tot}}(\boldsymbol{r},t)}{\partial t}=\frac{1}{\epsilon_{\mathrm{eff}}(\boldsymbol{r})}[\boldsymbol{\nabla}\times\boldsymbol{H}_{\mathrm{tot}}(\boldsymbol{r},t)-\boldsymbol{J}_{\mathrm{tot}}(\boldsymbol{r},t)], \tag{4}$$

$$\frac{\partial \boldsymbol{H}_{\mathrm{tot}}(\boldsymbol{r},t)}{\partial t}=-\frac{1}{\mu_0}\boldsymbol{\nabla}\times\boldsymbol{E}_{\mathrm{tot}}(\boldsymbol{r},t), \tag{5}$$

$$\frac{\partial \boldsymbol{J}_p(\boldsymbol{r},t)}{\partial t}=\alpha(\boldsymbol{r})\boldsymbol{J}_p(\boldsymbol{r},t)+\beta(\boldsymbol{r})\boldsymbol{E}_{\mathrm{tot}}(\boldsymbol{r},t). \tag{6}$$

Note that in Eq. (6) the evolved current is only due to the metal (i.e., nonmolecular current), but the electric field is the *total* field from the vacuum, metal, and molecule. The molecular current $\boldsymbol{J}_m$ depends on the wave function and is derived in Sec. II B.

We introduce the position-dependent (i.e., material-dependent) expressions [see Eq. (2.2) in Ref. 26],

$$\epsilon_{\mathrm{eff}}(\boldsymbol{r})=\epsilon_0\epsilon_{r,\infty}(\boldsymbol{r}), \tag{7}$$

$$\alpha(\boldsymbol{r})=-\gamma_D(\boldsymbol{r}), \tag{8}$$

$$\beta(\boldsymbol{r})=\epsilon_0[\omega_D(\boldsymbol{r})]^2, \tag{9}$$

where $\epsilon_{r,\infty}(\boldsymbol{r})$, $\gamma_D(\boldsymbol{r})$, and $\omega_D(\boldsymbol{r})$ are the standard Drude asymptotic relative permittivity, damping constant, and plasma frequency, respectively. In practice, these values are fitted to experiment over a finite frequency range of interest.[25,26,30]

For compactness, the explicit $\boldsymbol{r}$ and t dependence is henceforth generally dropped. For the magnetic field, recall that $\boldsymbol{H}_p=\boldsymbol{H}_{\mathrm{tot}}-\boldsymbol{H}_m$ (and likewise for $\boldsymbol{E}_p$ and $\boldsymbol{J}_p$) which yields

$$\frac{\partial \boldsymbol{H}_p}{\partial t}=\frac{\partial \boldsymbol{H}_{\mathrm{tot}}}{\partial t}-\frac{\partial \boldsymbol{H}_m}{\partial t}=-\frac{1}{\mu_0}\boldsymbol{\nabla}\times\boldsymbol{E}_{\mathrm{tot}}+\frac{1}{\mu_0}\boldsymbol{\nabla}\times\boldsymbol{E}_m,$$

and therefore,

$$\frac{\partial \boldsymbol{H}_p}{\partial t}=-\frac{1}{\mu_0}\boldsymbol{\nabla}\times\boldsymbol{E}_p. \tag{10}$$

For the electric field,

$$\frac{\partial \boldsymbol{E}_p}{\partial t}=\frac{\partial \boldsymbol{E}_{\mathrm{tot}}}{\partial t}-\frac{\partial \boldsymbol{E}_m}{\partial t}$$

$$=\frac{1}{\epsilon_{\mathrm{eff}}}(\boldsymbol{\nabla}\times\boldsymbol{H}_{\mathrm{tot}}-\boldsymbol{J}_{\mathrm{tot}})-\frac{1}{\epsilon_0}(\boldsymbol{\nabla}\times\boldsymbol{H}_m-\boldsymbol{J}_m),$$

and since $\boldsymbol{J}_{\mathrm{tot}}=\boldsymbol{J}_p+\boldsymbol{J}_m$, we get

$$\frac{\partial \boldsymbol{E}_p}{\partial t}=\frac{1}{\epsilon_{\mathrm{eff}}}\boldsymbol{\nabla}\times\boldsymbol{H}_p+\left(\frac{1}{\epsilon_{\mathrm{eff}}}-\frac{1}{\epsilon_0}\right)\boldsymbol{\nabla}\times\boldsymbol{H}_m$$

$$-\frac{1}{\epsilon_{\mathrm{eff}}}(\boldsymbol{J}_p+\boldsymbol{J}_m)+\frac{1}{\epsilon_0}\boldsymbol{J}_m. \tag{11}$$

Finally, note that $1/\epsilon_{\mathrm{eff}}-1/\epsilon_0=0$ for the molecular current

terms since $\epsilon_{\text{eff}}=\epsilon_0$ in the vacuum where the molecule is embedded (i.e., not directly on the metal). Thus,

$$\frac{\partial \boldsymbol{E}_p}{\partial t}=\frac{1}{\epsilon_{\text{eff}}}\boldsymbol{\nabla}\times\boldsymbol{H}_p+\left(\frac{1}{\epsilon_{\text{eff}}}-\frac{1}{\epsilon_0}\right)\boldsymbol{\nabla}\times\boldsymbol{H}_m-\frac{1}{\epsilon_{\text{eff}}}\boldsymbol{J}_p. \quad (12)$$

B. Molecular part

Now, we derive expressions for the evolution of the fields and current due to the molecule. The electric and magnetic fields are straightforward, as they are simply fields in a vacuum with a source,

$$\frac{\partial \boldsymbol{E}_m}{\partial t}=\frac{1}{\epsilon_0}[\boldsymbol{\nabla}\times\boldsymbol{H}_m-\boldsymbol{J}_m], \quad (13)$$

$$\frac{\partial \boldsymbol{H}_m}{\partial t}=-\frac{1}{\mu_0}\boldsymbol{\nabla}\times\boldsymbol{E}_m. \quad (14)$$

To calculate the current on the molecule we first use a linear Hamiltonian. The von Neumann equation for the time evolution of the density matrix $\rho(t)$ is given by

$$i\frac{\partial \rho(t)}{\partial t}=[H_0,\rho(t)]+[\boldsymbol{\mu}_m\cdot\boldsymbol{E}_p(\boldsymbol{r}_m,t),\rho(t)]-i\gamma_m\rho(t), \quad (15)$$

where $\boldsymbol{r}_m$ is the location of the molecule, H_0 is the Hamiltonian for the molecule in the absence of a field, $\boldsymbol{\mu}_m$ is the dipole moment of the molecule, and γ_m is a term describing the phenomenological damping of the molecule's oscillations. Note that the molecule's dipole moment couples to $\boldsymbol{E}_p(\boldsymbol{r}_m,t)$, which is the external field (described above) at the position of the molecule.

For a two-level system, the expression (in a.u.) for the $\rho_{21}(t)$ element is then

$$i\frac{\partial \rho_{21}(t)}{\partial t}=\omega_m\rho_{21}(t)+\boldsymbol{\mu}_{21}\cdot\boldsymbol{E}_p(\boldsymbol{r}_m,t)-i\gamma_m\rho_{21}, \quad (16)$$

where ω_m is the difference in energies of states 1 and 2. As is regularly done in RPA, we introduce the real and imaginary parts of $\rho_{21}(t)$,

$$X(t)\equiv \text{Re}[\rho_{21}(t)], \quad (17)$$

$$Y(t)\equiv \text{Im}[\rho_{21}(t)]. \quad (18)$$

Equation (16) is then solved by evolving $X(t)$ and $Y(t)$ separately,

$$\frac{\partial X(t)}{\partial t}=\omega_m Y(t)-\gamma_m X(t), \quad (19)$$

$$\frac{\partial Y(t)}{\partial t}=-\omega_m X(t)-\gamma_m Y(t)-\boldsymbol{\mu}_m(t)\cdot\boldsymbol{E}_p(\boldsymbol{r}_m,t). \quad (20)$$

Finally, the current on the molecule is calculated according to [see Eq. (B2) in Ref. 1),

$$\boldsymbol{J}_m(\boldsymbol{r},t)=\boldsymbol{j}_m(t)\,\delta(\boldsymbol{r}-\boldsymbol{r}_m), \quad (21)$$

where

$$\boldsymbol{j}_m(t)=\sum_{ij}\boldsymbol{j}_{ij}\rho_{ij}(t) \quad (22)$$

$$=[\boldsymbol{j}_{12}\rho_{12}(t)+\boldsymbol{j}_{21}\rho_{21}(t)]. \quad (23)$$

The matrix element $\boldsymbol{j}_{12}$ is evaluated according to

$$\boldsymbol{j}_{12}=\langle\psi_2|\hat{\boldsymbol{j}}|\psi_1\rangle \quad (24)$$

$$=-i\langle\psi_2|\,\boldsymbol{\nabla}\,|\psi_1\rangle \quad (25)$$

$$=-i\omega_m\boldsymbol{\mu}_m, \quad (26)$$

and similarly, $\boldsymbol{j}_{21}=i\omega_m\boldsymbol{\mu}_m$. From this, we get that the total molecular current is

$$\boldsymbol{j}_m(t)=[\boldsymbol{j}_{12}\rho_{12}(t)+\boldsymbol{j}_{21}\rho_{21}(t)] \quad (27)$$

$$=i\omega_m\boldsymbol{\mu}_m[\rho_{21}(t)-\rho_{12}(t)], \quad (28)$$

and since $\rho_{12}=\rho_{21}^*=X-iY$ we get, upon simplification, the final equation for the molecular current

$$\boldsymbol{j}_m(t)=-2\omega_m\boldsymbol{\mu}_m Y(t). \quad (29)$$

C. Localized source structure

The spatial three-dimensional delta function in Eq. (21) is evaluated by discretization; the molecule is placed at the center point of a Yee voxel, so that the delta function becomes $0.25dV$ on the set of the four nearest points, where dV is the volume of each voxel.

For concreteness, if the molecule is at the center of the voxel with grid indices (i,j,k), its position in space will be $\boldsymbol{r}_m=(idx,jdy,kdz)+\frac{1}{2}(dx,dy,dz)$. Since the currents lie on the same grid as the electric field, as opposed to the magnetic field which is the other interlaced grid in FDTD, the delta function also lies on the electric field grid. The positions in space of the x-components of the delta function are then $(idx,jdy,kdz)+(\frac{1}{2}dx,0,0)$, and similarly for the y- and z-components.

Now, the four nearest x-components to $\boldsymbol{r}_m$ have grid indices: (i,j,k), $(i,j,k+1)$, $(i,j+1,k)$, and $(i,j+1,k+1)$. Thus, the x-component of the delta function is equal to $0.25dV$ at these four grid points, which lie on the $\boldsymbol{E}_x/\boldsymbol{J}_x$ grid, and zero elsewhere. Similarly, the four nearest points for the y-component are (i,j,k), $(i,j,k+1)$, $(i+1,j,k)$, and $(i+1,j,k+1)$; and the four nearest points for the z-component are (i,j,k), $(i,j+1,k)$, $(i+1,j,k)$, and $(i+1,j+1,k)$.

One important caveat is that these grid points all must be in the vacuum, as the formalism is only valid for an isolated point source. This delta function approach, therefore, cannot be used in system where the molecule is very close (within a grid spacing) to a metal surface; an alternate approach capable of handling this situation is outlined in Sec. IV.

D. Combined FDTD-RPA scheme

The combined FDTD-RPA scheme evolves eight quantities in time: the fields due to the molecule $(\boldsymbol{E}_m,\boldsymbol{H}_m,\boldsymbol{J}_m)$, the real and imaginary parts of the density matrix (X,Y), and the fields due to the vacuum and metals $(\boldsymbol{E}_p,\boldsymbol{H}_p,\boldsymbol{J}_p)$. The relevant evolution expressions for the vacuum and metal parts of the fields/currents are Eqs. (10), (12), and (6). The expres-

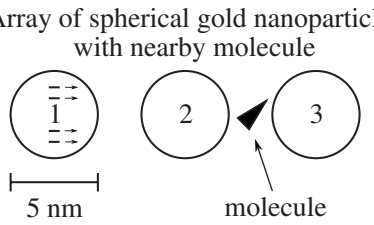

FIG. 1. The system consists of a line of three spherical gold nanoparticles all with radii of 2.5 nm, and center-to-center separation of three times the radius (7.5 nm). There is a northwest (i.e., *xy*) oriented molecule located midway between the second and third nanoparticle (molecule size not to scale). The system is initialized with a uniform *x*-oriented current on nanoparticle 1. The background is the vacuum.

sions for the molecular fields are Eqs. (13), (14), and (29), while the evolution of the density matrix is given by Eqs. (19) and (20).

For the FDTD simulations, we use a simple cubic Yee lattice,[25,31] and in order to remove spurious reflections of the fields from the edges of the grid, we apply an absorbing boundary condition (ABC), by multiplying the fields by a space-dependent function $f(\boldsymbol{r})$ after each time step, similar to Ref. 26. For example, in one dimension on the right side of the grid this function takes the form,

$$f(x) = \begin{cases} 1, & x < x_{\max} - w \\ \exp\left[-\dfrac{(x - x_{\max} + w)^2}{(-w^2/\ln h)} \right], & x \geq x_{\max} - w. \end{cases} \tag{30}$$

Here, w is the width of the ABC in a.u. and h is the "height" the ABC (i.e., the value of the ABC at the grid edge) which ranges between (0,1). The particular numerical simulation parameters are discussed in Sec. III. An alternative is to use the perfectly matched layers approach, as discussed in Ref. 25.

III. RESULTS

We applied the combined FDTD-RPA approach to three collinear spherical gold nanoparticles with a dipolar molecule located between the second and third, as shown in Fig. 1. The background is taken to be the vacuum, as the substrate is expected to have a small effect on the qualitative features of the system. The electrical and potentially magnetic properties of a real substrate, however, are straightforward to include in the formalism and would be required to accurately model a real device. The spheres all have a radius of $b = 2.5$ nm, and the center-to-center separation is $3b = 7.5$ nm. The molecule points along the *xy*-direction and has a dipole moment of 8 a.u., which is roughly 20 D; in the future we will study localized collections of molecules which together have very large dipole moments. The molecule's natural frequency (ω_m) was chosen to be 0.0941 a.u. (2.54 eV) such that it occurs near the surface plasmon absorbance of the metal nanoparticles in the array. The molecular damping parameter was taken as $\gamma_m = 0.001$ a.u. The Drude parameters for gold were taken from Ref. 30. For a comprehensive list of the Drude parameters, as well as the relevant molecular parameters, refer to Table I.

TABLE I. The physical parameters for gold and for the molecule. All values with units are in a.u.

Gold	Molecule
$\omega_D = 0.3298$	$\omega_m = 0.0941$
$\gamma_D = 0.0279$	$\gamma_m = 0.0010$
$\epsilon_{r,\infty} = 9.068$	$\mu_m = 8$

For each simulation, the total volume was approximately $42 \times 26 \times 26$ nm^3, with a grid spacing of $dx = dy = dz = 0.53$ nm, and 200 000 total grid points, including an ABC of width 2.6 nm on all edges of the grid. The time step was taken to be 0.9 times the Courant stability limit,[25] which corresponds to 0.038 a.u. $\approx 10^{-3}$ fs. To ensure all fields decayed to zero, we ran each simulation for 5000 a.u. (121 fs), which required roughly 130 000 time steps and took about 1 h on a 3 GHz microprocessor. The complete list of simulation parameters, including grid, time step, ABC, etc., is shown in Table II.

The system was initialized by starting a uniform *x*-polarized current on the first nanoparticle, which physically corresponds to a localized surface plasmon excitation on this nanoparticle. The total current on nanoparticle 1 is taken to be $J^{\text{tot}}_{x,1}(t=0) = 0.5$ a.u. Although this setup is not realistic, it allows us to elucidate the energy transfer effects of the array by measuring the induced total currents on the other particles in the array. For example, the total current on nanoparticle k at time t is simply

$$J^{\text{tot}}_{x,k}(t) = \int_{\text{NP } k} J^{\text{tot}}_x(\boldsymbol{r},t) d^3\boldsymbol{r}. \tag{31}$$

In particular, we measure the energy transfer between the second and third nanoparticles by comparing their relative total currents.

A. Array without molecule

First we investigate some of the transfer properties of the array without a molecule. Figure 2 shows the total *x* and *y* currents on the third nanoparticle as a function of time. As expected, the current oscillations are roughly dipolar and decay due to the Drude damping in the gold. The envelope of the current oscillations begins roughly 80 a.u. (~2 fs) into the simulation, and given a center-to-center distance of $6b = 15$ nm between the first nanoparticle, where we started the current, and the third nanoparticle, this corresponds to an approximate group velocity of $0.03c$. Also, note the small nonzero *y* current on the third nanoparticle. This nonphysical current is an artifact of the discrete grid; we verified that the *y* current converges to zero with decreased grid spacing.

TABLE II. The simulation parameters. All values with units are in a.u.

Grid	Time	Absorbing boundary
$N_x = 80$		
$N_y = 50$	$dt = 0.0379$	$w = 50$
$N_z = 50$	$t_{\max} = 5000$	$h = 0.2$
$dx = dy = dz = 10$		

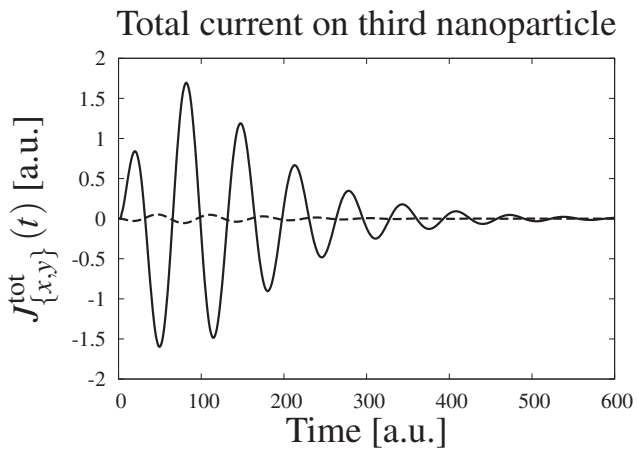

FIG. 2. The total x (solid) and y (dashed) polarized currents on the third nanoparticle as a function of time for the array without a molecule. It takes approximately 2 fs for the pulse envelope to reach this nanoparticle, which corresponds to an approximate localized SPP group velocity of $0.03c$. The small y-current is nonphysical and is due to the finite grid spacing.

B. Array with molecule

Next we place a dipolar molecule between the second and third nanoparticles (see Fig. 1). The electric field between the second and third molecule induces a dipolar electronic oscillation in the molecule (Fig. 3). The decay of the time signal and the corresponding width of the frequency signal are due to the damping on the molecule and the energy transfer to the nearby metal, which also damps away the energy. The frequency-resolved current induced on the molecule, $J_m(\omega)$, shows that the resonance peak of the molecule, denoted by $\tilde{\omega}_m$, occurs at approximately 2.54 eV and is thus redshifted from $\omega_m = 2.56$ eV (both shown as arrows in Fig. 3). Note that frequency-resolved currents are obtained from the Fourier transform of the time-resolved total current,

$$J_x^{\mathrm{tot}}(\omega) = \frac{1}{2\pi}\int_0^\infty J_x^{\mathrm{tot}}(t)e^{-i\omega t}dt. \tag{32}$$

In all plots we leave current values in a.u., but as is customary we express energies (i.e., frequencies) in eV.

Of particular interest is how this molecular excitation affects transfer along the array. Figure 4 shows the ratio of the frequency-resolved x-currents on nanoparticles 2 and 3, both with and without a molecule present. This quantity, denoted

$$T^x_{2\to 3}(\omega) \equiv \left|\frac{J^{\mathrm{tot}}_{x,3}(\omega)}{J^{\mathrm{tot}}_{x,2}(\omega)}\right|, \tag{33}$$

is a good measure of the percent of x-polarized energy that is transferred from the second nanoparticle to the third. Without a molecule, the percent energy transfer varies with frequency and ranges between 13% and 20% over the frequency range shown. With a molecule, however, there is a enhancement of transfer for frequencies lower than the molecule's resonance $\tilde{\omega}_m$ (shown as an arrow) and a decreased transfer effect for higher frequencies.

This decreased transfer occurs largely because, over this frequency range, the molecule scatters the incident x-polarized energy into y-polarized energy, as shown in Fig. 5. Here, the frequency-resolved x-current on the third nanoparticle shows a dip at a frequency above the molecule's resonance peak $\tilde{\omega}_m$ (shown as an arrow) and a peak at a frequency below. The locations of the dip and peak are

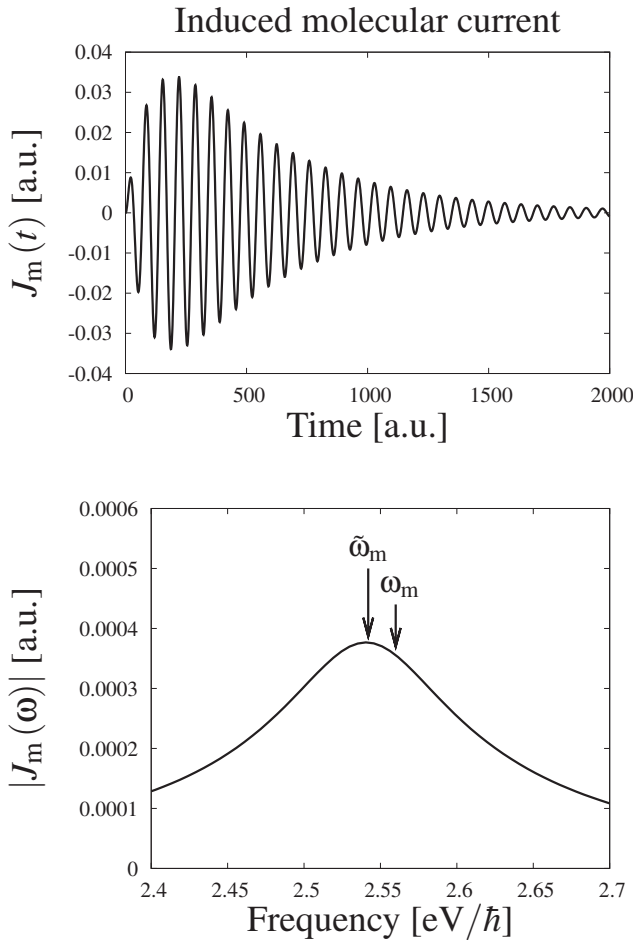

FIG. 3. The time-resolved (top) and frequency-resolved (bottom) currents on the molecule. Under the electric field, the resonance peak of the molecule ($\tilde{\omega}_m$) is approximately 2.54 eV and is, therefore, redshifted from the molecule's natural frequency (ω_m) of 2.56 eV.

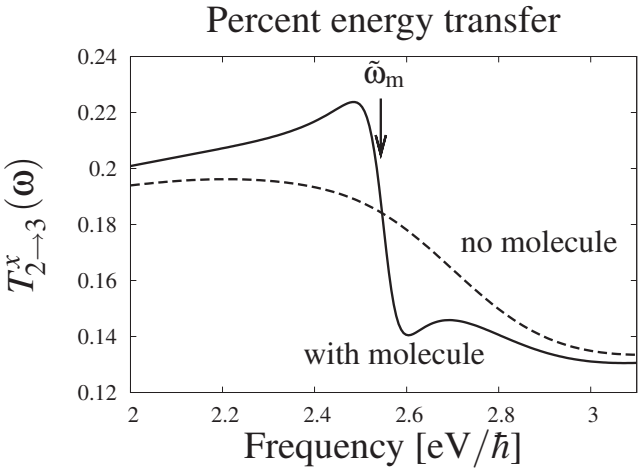

FIG. 4. The approximate percent x-polarized energy transfer between nanoparticles 2 and 3, both without a molecule (dashed) and with a molecule (solid). In the presence of a molecule, the transfer is enhanced for frequencies below the molecule's resonance ($\tilde{\omega}_m$), while for frequencies above it is diminished due to scattering to the y-polarization.

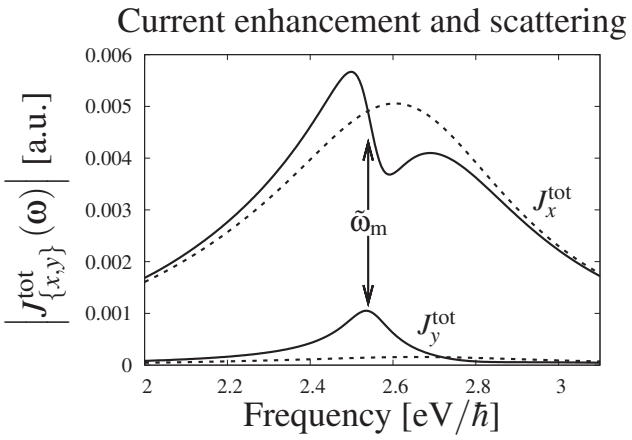

FIG. 5. The x-polarized (top two curves) and y-polarized (bottom two curves) frequency-resolved total currents on the third nanoparticle, both without the molecule (dashed) and with the molecule present (solid). In the presence of a molecule the spectrum shows a characteristic interference peak and dip, which are symmetric around the molecular resonance ($\tilde{\omega}_m$). The dip arises from the xy-oriented molecule scattering the initially x-polarized electromagnetic energy to the y-polarization.

roughly symmetric around $\tilde{\omega}_m$ and probably due to interference, i.e., a Fano-type effect.[32,33] Additionally, the magnitude of the y-current around the resonance frequency is drastically increased; at $\tilde{\omega}_m$, the magnitude of the y-current is approximately 20% of the x-current. Thus, the molecule partially scatters the incident x-polarized energy into y-polarized energy. These results agrees with the results shown in Fig. 4 where the x-polarized transfer efficiency was decreased (i.e., scattered to y).

The physical origin of the $x \rightarrow y$ scattering is made clear when we directly observe the strong effect the molecule has on the time-dependent electric fields in the system. Figure 6 shows three time slices of the y-polarized electric field in the system, as a function of x and y at fixed $z=0$, both without a molecule (top), and with a molecule (bottom). For these particular results only, we took a finer grid spacing of $dx=dy=dz=5$ a.u. in order to generate clearer pictures. Blue shades are positive values and red shades are negative. The y-part of the oscillating dipolar electric field around each nanoparticle is clearly visible (blue $\rightarrow$ red $\rightarrow$ blue). There is a strong localized oscillating dipolar field around the molecule, which serves to significantly enhance the field between the

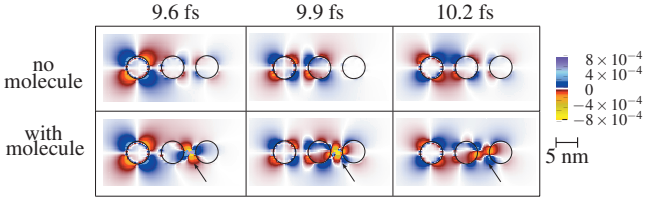

FIG. 6. (Color) Three snapshots in time of the y-component of the electric field with (bottom) and without (top) a molecule. Shades of blue are positive values, while shades of red are negative values. The fields around the metal nanoparticles are essentially those of oscillating dipoles. The strong northwest-oriented oscillating dipolar field around the molecule is visible between the second and third nanoparticles (denoted by an arrow). This dipolar molecular field serves to scatter the x-polarized energy (not shown) into y-polarized energy. The figure has been cropped to focus on the region around the array, and the scale bar is in a.u.

second and third nanoparticles (denoted by an arrow), and thus induce y-polarized currents at the surface of the third nanoparticle.

In essence, the molecule absorbs electromagnetic energy from the array and then radiates at a slightly different frequency. This radiated energy is then absorbed by the nearby nanoparticle. The net effect is that even though the damping on the molecule serves to lower the overall energy in the system as compared to the case without the molecule, there is a strong enhancement of currents on the last nanoparticle. This scattering effect is qualitatively similar to our previous numerical results which were based on a simplified point-plasmon array interacting with a molecule.[1] Since this effect varies strongly with the molecule's orientation and position, the array acts as a type of chemical sensor. Additionally, one can envisage building a plasmonic switch wherein the orientation of the molecule gates transfer into different output paths.[1]

These results epitomize the two fundamental directions of plasmon/molecule interaction in nanopolaritonics: namely, the plasmons affect the molecule by inducing electronic oscillations (Fig. 3), and the molecule in turn significantly affects the transfer of the plasmons (Fig. 5) through near-field interactions (Fig. 6).

IV. FUTURE PROSPECTS: BEYOND LOCALIZED TWO-LEVEL RPA

Going beyond the localized linearized RPA two-level description will be quite simple. The full Schrödinger equation for the wave function is

$$i\frac{\partial \Psi}{\partial t} = H\Psi, \tag{34}$$

or in von Neumann matrix form, essentially

$$i\frac{\partial \rho(t)}{\partial t} = [H, \rho(t)] - i\gamma_m \rho(t), \tag{35}$$

where

$$H = H_0 + \mu_m(\boldsymbol{E}_p + \boldsymbol{E}_m) + V_{\mathrm{xc}}, \tag{36}$$

where we have introduced the zeroth-order Hamiltonian and the exchange-correlation potential. For the purpose of driving $\boldsymbol{E}_m$ and $\boldsymbol{H}_m$, the description of a current as a delta function is appropriate. For the purpose of acting on the molecule itself, however, the molecule-induced electric field will be calculated, in practice, as a Coulomb term with a possible current-induced correction,

$$\boldsymbol{E}_m(\boldsymbol{r},t) = \nabla\Phi_m - \frac{1}{c}\frac{\partial \boldsymbol{A}_m}{\partial t}, \tag{37}$$

where we introduced the scalar and vector potentials in terms of the electron density n,

$$\Phi_m(\boldsymbol{r},t) = \int \frac{n(\boldsymbol{r}',t')}{|\boldsymbol{r}-\boldsymbol{r}'|} d^3\boldsymbol{r}', \tag{38}$$

$$\boldsymbol{A}_m(\boldsymbol{r},t) = -\frac{4\pi}{c}\int \frac{\boldsymbol{J}_m(\boldsymbol{r}',t')}{|\boldsymbol{r}-\boldsymbol{r}'|}d^3\boldsymbol{r}, \tag{39}$$

and t' is the retarded time,

$$t' = t - |\boldsymbol{r}-\boldsymbol{r}'|/c. \tag{40}$$

The integral in Eq. (39) is simple to evaluate since the source term is localized in space.

The more accurate description of the molecule-induced electric field will also be useful on a tip which is sufficiently close to the molecule such that the delta function cannot be used. In practice there should be a transition region where the field changes smoothly from the analytical form to the FDTD form.

Finally, an interesting question is how to handle multiple molecules distributed over a large region. One option is to use multiple regions, each with its own electric field grids; the other, more interesting option is to use a single molecule-based electric field, but eliminate analytically the electric field contribution for each of the fields. Schematically, the electric field due to the molecules will be calculated as:

$$\boldsymbol{E}_m(\boldsymbol{r},t) = \boldsymbol{E}_m^{\text{Maxwell}}(\boldsymbol{r},t) + \boldsymbol{E}_{\text{partial}}^{\text{analytical}} - \boldsymbol{E}_{\text{partial}}^{\text{Maxwell}}, \tag{41}$$

where the "Maxwell" superscript refers to a numerical solution to Eq. (13), the analytical refers to Eq. (37), and the "partial" subscript refers to the consideration of a small region located near the molecule. This approach is viable because the numerical solution of $\boldsymbol{E}_{\text{partial}}^{\text{Maxwell}}$ is possible analytically if the magnetic contribution is ignored. Details and applications will be presented in future publications.

V. CONCLUSIONS

In summary, we have developed a split field FDTD-RPA formalism for combined metal/molecule systems based on linear response for the molecule. Numerical studies of a linear array of three gold nanoparticles with an *xy*-oriented molecule between the second and third demonstrate the ability of a dipolar molecule to either enhance transmission of *x*-polarized SPPs through the array, or to scatter incident *x*-polarized SPPs to the *y*-polarization. These results are qualitatively similar to previously published simulation results,[1] but show an enhanced effect.

There are many extensions to these results, which we will pursue in the future. The most obvious improvement is to go beyond linear response, as discussed in Sec. IV. Since linear response is expected to break down in regions of intense electric fields, this approach will be suitable for modeling interactions of molecules with nanoscale energy focusing devices, such as tips, or near highly excited metal structures. This, in turn, will enable the formalism to capture interesting nonlinear effects, such as multiharmonic emission from molecules under strong fields.

ACKNOWLEDGMENTS

This work was supported by NSF Grant No. CHE-0810003. Discussions with Niri Govind are gratefully acknowledged.

[1] D. Neuhauser and K. Lopata, J. Chem. Phys. **127**, 154715 (2007).
[2] E. Ozbay, Science **311**, 189 (2006).
[3] S. A. Maier and H. A. Atwater, J. Appl. Phys. **98**, 011101 (2005).
[4] S. Nie and S. R. Emory, Science **275**, 1102 (1997).
[5] C. L. Haynes, C. R. Yonzon, X. Zhang, and R. P. V. Duyne, J. Raman Spectrosc. **36**, 471 (2005).
[6] C. E. Talley, J. B. Jackson, C. Oubre, N. K. Grady, C. W. Hollars, S. M. Lane, T. R. Huser, P. Nordlander, and N. J. Halas, Nano Lett. **5**, 1569 (2005).
[7] K. T. Shimizu, W. K. Woo, B. R. Fisher, H. J. Eisler, and M. G. Bawendi, Phys. Rev. Lett. **89**, 117401 (2002).
[8] J. Lee, A. Govorov, J. Dulka, and N. Kotov, Nano Lett. **4**, 2323 (2004).
[9] B. N. J. Persson and N. D. Lang, Phys. Rev. B **26**, 5409 (1982).
[10] T. Jennings, M. Singh, and G. Strouse, J. Am. Chem. Soc. **128**, 5462 (2006).
[11] A. O. Govorov, G. W. Bryant, W. Zhang, T. Skeini, J. Lee, N. A. Kotov, J. M. Slocik, and R. R. Naik, Nano Lett. **6**, 984 (2006).
[12] J. Dintinger, S. Klein, F. Bustos, W. L. Barnes, and T. W. Ebbesen, Phys. Rev. B **71**, 035424 (2005).
[13] F. D. Stefani, K. Vasilev, N. Bocchio, N. Stoyanova, and M. Kreiter, Phys. Rev. Lett. **94**, 023005 (2005).
[14] G. Colas des Francs, C. Girard, T. Laroche, G. Lévèque, and O. J. F. Martin, J. Chem. Phys. **127**, 034701 (2007).
[15] S. Corni and J. Tomasi, J. Chem. Phys. **117**, 7266 (2002).
[16] R. S. Swathi and K. L. Sebastian, J. Chem. Phys. **126**, 234701 (2007).
[17] U. Kreibig and M. Vollmer, *Optical Properties of Metal Clusters* (Springer-Verlag, Berlin, 1994).
[18] M. Quinten, A. Leitner, J. R. Krenn, and F. R. Aussenegg, Opt. Lett. **23**, 1331 (1998).
[19] B. T. Draine and P. J. Flatau, J. Opt. Soc. Am. A Opt. Image Sci. Vis. **11**, 1491 (1994).
[20] E. Hao and G. C. Schatz, J. Chem. Phys. **120**, 357 (2004).
[21] R. Baer, K. Lopata, and D. Neuhauser, J. Chem. Phys. **126**, 014705 (2007).
[22] K. Lopata, D. Neuhauser, and R. Baer, J. Chem. Phys. **127**, 154714 (2007).
[23] E. Prodan, C. Radloff, N. J. Halas, and P. Nordlander, Science **302**, 419 (2003).
[24] E. Prodan and P. Nordlander, J. Chem. Phys. **120**, 5444 (2004).
[25] A. Taflove and S. Hagness, *Computational Electrodynamics: The Finite-Difference Time-Domain Method* (Artech House, Boston, 2005).
[26] S. K. Gray and T. Kupka, Phys. Rev. B **68**, 045415 (2003).
[27] S. A. Maier, P. G. Kik, and H. A. Atwater, Appl. Phys. Lett. **81**, 1714 (2002).
[28] W. Zhang, A. O. Govorov, and G. W. Bryant, Phys. Rev. Lett. **97**, 146804 (2006).
[29] A. K. Gupta and D. Neuhauser, Int. J. Quantum Chem. **81**, 260 (2001).
[30] A. Vial, A.-S. Grimault, D. Macías, D. Barchiesi, and M. L. de la Chapelle, Phys. Rev. B **71**, 085416 (2005).
[31] K. Yee, IEEE Trans. Antennas Propag. **14**, 302 (1966).
[32] D. Neuhauser, T.-J. Park, and J. I. Zink, Phys. Rev. Lett. **85**, 5304 (2000).
[33] K. Lopata and D. Neuhauser (unpublished).